The role of acoustofluidics in targeted drug delivery

Nilanjana Bose, Xunli Zhang, Tapas K. Maiti, and Suman Chakraborty

Citation: Biomicrofluidics **9**, 052609 (2015); doi: 10.1063/1.4928947
View online: http://dx.doi.org/10.1063/1.4928947
View Table of Contents: http://scitation.aip.org/content/aip/journal/bmf/9/5?ver=pdfcov
Published by the AIP Publishing

The role of acoustofluidics in targeted drug delivery

Nilanjana Bose,[1] Xunli Zhang,[2] Tapas K. Maiti,[1] and Suman Chakraborty[3,a)]
[1]*Department of Biotechnology, Indian Institute of Technology Kharagpur, Kharagpur 721302, India*
[2]*Bioengineering Group, Engineering Sciences, University of Southampton, Southampton SO17 1BJ, United Kingdom*
[3]*Department of Mechanical Engineering, Indian Institute of Technology Kharagpur, Kharagpur 721302, India*

(Received 1 June 2015; accepted 8 August 2015; published online 20 August 2015)

With the fast development of acoustic systems in clinical and therapeutic applications, acoustically driven microbubbles have gained a prominent role as powerful tools to carry, transfer, direct, and target drug molecules in cells, tissues, and tumors in the expanding fields of targeted drug delivery and gene therapy. The aim of the present study is to establish a biocompatible acoustic microfluidic system and to demonstrate the generation of an acoustic field and its effects on microbubbles and biological cells in the microfluidic system. The acoustic field creates non-linear oscillations of the microbubble-clusters, which results in generation of shear stress on cells in such microsystems. This effectively helps in delivering extracellular probes in living cells by sonoporation. The sonoporation is investigated under the combined effects of acoustic stress and hydrodynamic stress during targeted drug and gene delivery. © *2015 AIP Publishing LLC*.
[http://dx.doi.org/10.1063/1.4928947]

I. INTRODUCTION

Ultrasound has been used to image tissue borders, such as cardiac chamber, ventricular wall, and normal liver, spleen, or kidney. However, there are fundamental limitations on the ability of ultrasound alone to differentiate between healthy and diseased tissues, particularly when they are inside an organ and are not recognizable from surrounding tissues. Traditionally, small gas bubbles were used as echogenic particles to enhance ultrasound contrast, dated back to the 1960s,[1] in diagnostic imaging applications spanning cardiology and radiology by increasing the reflectivity of perfused tissues. Since then, microbubbles are widely used as Ultrasound Contrast Agents (UCA) in medical imaging,[2–8] owing to their capability of enhancing the reflection of ultrasound (US) waves.[9,10] Besides their use as contrast agents in diagnostics purposes, these microbubbles in conjunction with ultrasound have been off late used as a tool for targeted drug delivery and gene therapy.[11–16]

UCA or ultrasound contrast microbubbles are small (typically 1–8 μm in diameter) gas-filled microspheres and are coated with an adsorbed layer of proteins,[17] polymers,[18] or lipids.[19] Due to their highly echogenic nature, contrast microbubbles are capable of increasing the intensity of backscattered ultrasound to up to 20–30 dB.[20] Recently, a microbubble is engineered to load the therapeutic agent onto the shell to deliver a therapeutic payload into cancerous cells or a tumor and has been functionalized to carry targeting ligands[21] and genetic payloads.[22] Drug-loaded microbubbles are generally produced by incorporating the drugs during microbubble synthesis or by post-loading the drugs into or onto pre-formed microbubble.[23,24]

Fundamentally, ultrasound drives oscillations on and around microbubbles to induce large spatio-temporal velocity gradients, which, in turn, generates small-scale eddying forces, leading to a motion known as micro-streaming. Shear forces exerted by the acoustic micro-streaming

a)Author to whom correspondence should be addressed. Electronic mail: suman@mech.iitkgp.ernet.in

and the strain induced by a low-amplitude bubble oscillation have been used to manipulate the dynamics of vesicles, their deformations, and lysis.[25] Further, *in vitro* and *in vivo* insonation of contrast microbubbles in the presence of ultrasound could expand, move, or fragment microbubbles, thus resulting in the alterations in cell membrane and vascular permeability.[26–28] The continuous alteration of vascular or cellular permeability leads to drastically enhancing transient poration of blood vessels or cell membranes in a non-invasive manner. Cell membranes can open up temporary pores when subjected to ultrasound-microbubble impact, which get resealed[29] when the ultrasound is withdrawn. This is commonly known as reparable sonoporation.[30] There are several hypotheses to explain the sonoporation phenomenon such as push and pull mechanisms,[31] micro-jetting,[32] micro-streaming,[33] sonophore,[34] and as more recently proposed, translation of microbubbles through cells.[35] Although there are reports on *in vitro* sonoporation, the physical mechanisms underlying the sonoporation and its related biological effects have not been fully clarified, and challenges still remain to achieve controllable sonoporation outcomes associated with targeted drug delivery and gene therapy. In recent studies, therapeutic payloading by the oscillating microbubbles is being achieved using acoustics in microfluidic-based devices.[36]

In the present study, we have developed a biocompatible microfluidic device in which an ultrasonic standing wave (USW) is generated within the system. We have experimentally obtained the acoustic resonance modes of the microfluidic device which are chosen as the operating conditions for standing wave formation inside the microfluidic device. Experimental investigations have been focused on the formation of microbubble-clusters with these acoustic resonant frequencies in order to characterize the motion of the microbubble-clusters in such microdevice and their interactions with each other and with living cells. We have also theoretically analysed the shear stress generated by the oscillating microbubble-clusters which would be used as a tool to induce sonoporation in cardiomyoblast cells. Further, we have demonstrated the intracellular delivery of extracellular probe, propidium iodide in cardiomyoblast cells under the combined effects of acoustic stress and hydrodynamic stress.

II. THEORY

A. Establishing acoustophoresis in microfluidic system

Ultrasound is rapidly finding applications in MEMS-based devices such as controlling cell-cell interactions,[37] cell sorting,[38] and manipulation of cells and bioparticles in lab-on-a-chip systems.[39–41] It has been recognised as an alternative tool for microfluidic actuation primarily because of the availability of the wide ranges of length scales (wavelength) of the acoustics, among which ultrasound (typically characterised by acoustics with frequencies over 20 kHz) with frequencies of low MHz commensurate well with the length scales associated with typical microfluidic devices. The acoustic waves developed in microfluidic systems (though not limited to these systems) interact with reflected waves (either boundaries or reflectors) and interfere to form *stationary waves* or *standing waves*. Classically, such standing waves were demonstrated in Kundt's tube which is an experimental method to approximately determine the speed of sound. As the wavelength is inversely proportional to the frequency (the product being the speed of sound in that medium), operating at high frequencies ($\sim$MHz) requires a confined system in the sub-millimetre scale for effective manipulation of particles of the micron or sub-micron scales.

High intensity standing waves result in two important effects which are pivotal towards manipulation of fluids or particles—*acoustic streaming*[42] which imparts movement of the fluid in an acoustic field and *acoustic radiation*[43] force which exerts forces on suspended particles directed towards or away from nodes depending upon the compressibility of the medium. These two effects may be judiciously used in combination or separately for wide range of lab-on-a-chip applications and commonly known as *acoustophoresis*. It is important to mention in the context of the motion of particles, the drag force on the particles from the fluid is inevitable which limits the speed at which particles can be manipulated (e.g., separated) by the acoustic field. As the acoustic effects are dependent on the compressibility of the material, soft matters in the form of

microbubbles or biological cells behave distinctly different from rigid particles through their strong vibration response to the incoming acoustic waves owing to their compressible nature.

For a Newtonian fluid, the governing equation for the thermodynamics equation of state, the mass conservation or the continuity equation, and the Navier-Stokes equation may be described as

$$p = p(\rho), \tag{1a}$$

$$\frac{\partial \rho}{\partial t} + \nabla \cdot (\rho \mathbf{v}) = 0, \tag{1b}$$

$$\rho\left(\frac{\partial \mathbf{v}}{\partial t} + (\mathbf{v} \cdot \nabla)\mathbf{v}\right) = -\nabla p + \mu \nabla^2 \mathbf{v} + \left(\frac{\mu}{3} + \zeta\right)\nabla(\nabla \cdot \mathbf{v}), \tag{1c}$$

where p and ρ are the pressure and density of the medium, respectively, t is the time, $\mathbf{v}$ is the velocity vector, and μ and ζ are the first and second coefficient of viscosity assumed to be unaffected by other changes in the system. The compressible effect gives rise to the last term of Eq. (1c), the coefficient is typically expressed in terms of the viscosity ratio as $\beta_0 = (\mu/3 + \zeta)/\mu$.

Eqs. (1a)–(1c) represent coupled non-linear, partial differential equations which have analytical solutions only in limiting cases. The present situation may be analysed in the linearised framework valid under certain assumptions or approximations in the physical systems. The acoustic contributions to the pressure, density, and velocity fields are assumed to be small perturbations; Eqs. (1a)–(1c) may be expanded using:[44] $\rho = \rho_0 + \rho_1 + \rho_2$, $p = p_0 + p_1 + p_2$, and $\mathbf{v} = \mathbf{v}_0 + \mathbf{v}_1 + \mathbf{v}_2$ where the subscripts 0, 1, and 2 refer to the zero, first, and second order perturbations, respectively, to the governing equation. A quiescent fluid is subjected to acoustic effects should have $\mathbf{v}_0 = 0$.

Using the Taylor's series expansion of Eq. (1a) around $p_0 = p(\rho_0)$, the first order derivative may be expressed as $c_0^2 = \frac{\partial p}{\partial \rho}|_s$, where c_0 is the isentropic speed of the sound in the medium. The first order pressure may be represented as $p_1 = c_0^2 \rho_1$. The zero order solution of Eqs. (1a)–(1c) may be obtained as the hydrostatics of the system given by

$$-\nabla p_0 = 0;\ \partial/\partial t(\rho_0) = 0;\ \mathbf{v}_0 = 0, \tag{2}$$

which is satisfied by constant values of the pressure p_0 and ρ_0. Then, the solution to the first order for these quantities is obtained under the linearised approximation, assuming harmonic time dependence of the variables, in the inviscid limit may be described by Helmholtz equation as[41]

$$\nabla^2 p_1 = k_0^2 p_1, \tag{3}$$

where k_0 is the wave-number given by $k_0 = \omega/c_0$.

The liquid domain as described by Eq. (3) needs to be specified with a boundary condition. Depending upon the type of the solid substrate in contact with the liquid domain, there are three possibilities—soft-, hard-, and the lossy-wall boundary conditions. Soft wall condition is imposed when the solid medium in contact with the fluid is not able to sustain any pressure; described by the boundary condition—$p_1 = 0$. Typically, deformable walls of soft or deformable elastic materials like Poly-Di-Methyl-Siloxane (PDMS) walls, or free interfaces might be treated through this soft boundary condition. In such cases, the velocity at the PDMS boundary needs not to be zero. A hard-wall boundary condition is applied when the interfacing medium does not yield to the velocity of the liquid. As a result, the normal component of the velocity of the liquid at the wall is zero, which may be represented as $n \cdot \nabla p_1 = 0$. An ideal representation of the hard wall condition would be glass wall. However, in a more generic sense, a wall is more approximately represented as a lossy wall condition in view of the acoustic losses of the liquid to the surrounding medium; which may be described as $n \cdot \nabla p_1 = i\frac{\rho_0 \omega}{\rho_m c_m} p_1$, where the subscript m denotes the properties of the solid medium. The denominator $\rho_m c_m$ is known as the acoustic impedance of the medium. In the limiting case, when $\rho_m c_m \to 0$ or the acoustic

impedance is low, there is no loss or resistance at the interface and the same may be interpreted as soft wall condition. When $\rho_m c_m \rightarrow \infty$ or for very high impedance, the boundary is rigid or may be interpreted as hard wall condition. The speeds of sound in water and in PDMS are quite comparable. The attenuation of the acoustic energy in PDMS/water interface is 0.013 db/MHz/mm, which is much smaller than the attenuation at the glass/PDMS interface 0.7 dB/MHz/mm.[45] The ratio of the acoustic impedance of glass to that of the water is 13.2, whereas that of water to PDMS is 1.36. The resultant acoustic transmission of energy between water and PDMS may be obtained to be $\left(4\frac{Z_{PDMS}Z_{Water}}{(Z_{PDMS}+Z_{Water})^2}\right)$ as 97.6%. The acoustic impedance is much lower for air in comparison to the other materials.

When the incoming US enters into the bulk fluid, it travels in all the directions. It comes in the vicinity of the interface of the water and PDMS (three walls of the PDMS/glass hybrid microfluidic channel, while the fourth wall is glass). As discussed above, the attenuation of the acoustic energy is much lower in PDMS and the US waves move into the PDMS with a velocity similar to that of the water. The PDMS walls have some thickness and are open to the ambient on the other side. The US waves finally encounters the PDMS–air interface where some part of the wave gets reflected, some part gets absorbed, and rest gets transmitted to the air (see Fig. 1(b)). The reflected wave from the PDMS-air interface further moves along the PDMS and subsequently into the fluid. In this process, the incoming waves and the reflected waves interfere to form a standing wave inside the PDMS/glass hybrid microfluidic device. In glass microdevice, the ultrasound enters the microchannel and gets reflected from the other glass wall of the microchannel. The reflected and the incident waves superpose to form a standing wave inside the microdevice. A distinct difference of the glass microdevice from the PDMS/glass hybrid microfluidic device is that the fundamental modes in these two cases are different. The standing wave formed in the PDMS/glass hybrid microfluidic device has one-fourth wavelength in the fundamental mode, while in the glass microdevice, it is half the wavelength.

If the dimensions of the microfluidic channel are considered as (l, w, and h) corresponding to the length, width, and height, the resonant frequency of the standing wave may be represented analytically in the form

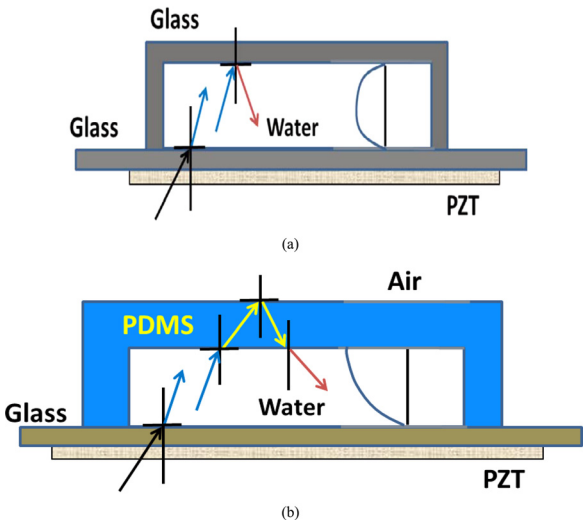

FIG. 1. The schematic of (a) the glass microdevice and (b) PDMS/glass hybrid microfluidic device; and how the ultrasound interacts with different interfaces to obtain standing waves. The arrows represent the acoustic waves generated from the piezo transducer (PZT) attached at the bottom of the glass surface in each of the devices with glycerol. When actuation matched the resonance condition in each of the microfluidic devices (resonance frequencies, $f_R = 2.37$ MHz and $f_R = 2.14$ MHz), a localized standing wave is generated above the transducer. The profiles are representatives of the superposed acoustic waves. The difference at the boundary of PDMS and glass surfaces comes from the soft and hard boundary conditions, respectively.

$$f_{nx,ny,nz} = \frac{c_w}{2}\sqrt{\frac{n_x^2}{l^2} + \frac{n_y^2}{w^2} + \frac{n_z^2}{h^2}}, \tag{4}$$

where n_x, n_y, and n_z are the (integer) resonance modes in three directions. *This frequency is independent of the type of the boundary condition imposed at the wall*. The resonance frequency and modes of operation for different microfluidic devices have been experimentally determined.

B. Acoustic radiation force on microbubbles

Particles in the form of gas bubbles, solid particles, or liquid drops suspended in an acoustically driven fluid undergo steady (time-averaged) hydrodynamic forces enabling them to demonstrate their ability to move in the suspended fluid, form clusters in certain regions, or interact with one another. These forces are called acoustic radiation forces or acoustic radiation pressure. These forces move the particles towards either the pressure nodes or the pressure antinodes depending on the density and compressibility of the particles and the medium. The incoming acoustic wave gets scattered from the particles which acts as a point-scatterer of acoustic waves (when the particle size is small compared to the wavelength of the acoustic waves). The radiation force originates from the superposition of the incident and the scattering waves in the medium. This radiation force sets up a gradient in the acoustic pressure near the particles. The motion of particles is not resolved to small time scales ($\sim\mu$m) which corresponds to the acoustic frequency ($\sim$MHz), and hence it is customary to consider the radiation force over a full oscillation cycle in an averaged sense.

Although particles in the form of gas bubbles experience the phenomenon as above, a distinctive feature of the gas bubble in liquid subjected to an acoustic wave is that it undergoes volume pulsations. The acoustic pressure gradient in conjunction with bubble oscillations can produce motion of the bubbles which is commonly known as Bjerknes force.[46] Conventionally, the forces on bubbles are divided depending upon either the force is from the incoming acoustic waves or from the scattered waves from other bubbles—*primary Bjerknes force* experienced by single/isolated bubbles and *secondary Bjerknes force* which considers the interactions of multiple bubbles.

The primary Bjerknes force acting on a single bubble of volume V in a field with pressure gradient ∇p_1 is given by $F_B = -\langle V(t)\nabla p_1(r,t)\rangle$, where F_B represents the force on the bubble and p_1 is the acoustic pressure in the medium at a position r in space and at a given time t. The notation $\langle\rangle$ represents averaged over a time period. Bubbles of equilibrium radius R_0 show a maximum response corresponding to its own resonance frequency f_b. Similarly, the driving or the input frequency also shows maximum response corresponding to a fixed bubble radius called resonance radius of the bubbles R_0, where the product of these two parameters is constant for bubble in air as $f_b R_0 = 3\,\mathrm{m/s}$.[47] For a standing wave established in space, bubbles of size less than resonance size travel to the pressure antinodes, and bubbles of greater than resonance size travel to the pressure nodes.[48] In other words, for a fixed equilibrium radius of the microbubble, the force is directed towards the pressure maximum if the bubble is driven below the resonance and towards the pressure minimum if driven above resonance.[49]

For multiple bubbles, under the assumptions of harmonically oscillating spherical bubbles, low pressure amplitude and large spacing between the bubbles, if the driving frequency lies between the two linear resonance frequencies of the individual bubbles, they will repel each other else they would get attracted. The resonance frequencies of the two bubble system also change as the bubbles approach each other.[50] Consequently, there is a phase shift between the bubble oscillations which may in turn lead to change in the mutual interaction force from attraction to repulsion. If the driving frequency is higher than the linear resonance frequency, the attractive force can turn to repulsive force when the bubbles come close to each other.[49] Contrary to this fact, two bubbles driven below their linear resonance frequencies can also suffer repulsion when nonlinear effect influences the interaction.[50] The magnitude of the breathing-mode resonance frequency is a function of the separation between the bubbles. The

sign of the force changes when the bubbles approach each other. The net force (secondary Bjerknes force) acting on a bubble from a second bubble in a time averaged sense is given by[51] $F_{B2} = -\frac{\rho}{4\pi r^2}\langle \dot{V}_1 \dot{V}_2 \rangle$, where ρ is the density of liquid, V_1 and V_2 are the volume of the two gas bubbles, and the force on the bubble is proportional to the rate of the change of the bubble volumes and inversely proportional to the square of the distance between the bubbles (r). If $\langle \dot{V}_1 \dot{V}_2 \rangle > 0$, the force is attractive and vice versa. When two bubbles attract and come close to each other, they may coincide to form a big bubble. Alternatively, if the bubbles have a gas protecting shell, then instead of collapsing, they tend to form a "grape" like aggregation of microbubbles into a single entity called *microbubble-cluster*.

III. EXPERIMENTAL METHODS

A. Materials and reagents

For glass-based microdevice, glass microcapillary was purchased from VitroCom (Ilkley, UK). Piezoelectric transducer (PZT) commonly known as PZ26 was composed of lead-zirconate-titanate material and was purchased from Ferroperm, Kvistgard, Denmark. For PDMS/glass hybrid microdevice fabrication, a negative photoresist SU-8-2075 was purchased from MicroChem Corp (MA, USA) and PDMS was purchased Sylgard 184 (Dow Corning, USA). Phosphate buffer salines (PBS), glycerol solution, were purchased from Sigma Aldrich (India). Dulbecco's Modified Essential Medium (DMEM), glutamine, penicillin, streptomycin, non-essential amino acids, fetal bovine serum, and trypsin-EDTA were purchased from Gibco (Gaithersburg, MD), and propidium iodide (PI) was purchased from Invitrogen (India). Optison™ Contrast Agents was purchased from GE Healthcare (Hatfield, UK).

B. Ultrasonic microfluidic device fabrication

A disposable glass microcapillary with dimensions—length = 25 mm, width = 6 mm, and height = 300 μm, is acoustically coupled to a PZT by means of a thin film of glycerol and the ultrasonic microfluidic device is generated. The PZT (length: 20 mm, width: 6 mm, and height: 1 mm) is held in place by a poly-methyl methacrylate (PMMA) spring loaded clamp (Fig. 1(a)) and driven by an RF power amplifier (240 L ENI, Rome, Italy) fed from a signal generator (Agilent, USA) to supply specific AC voltages of different amplitudes (A) and frequency (f). Alternatively, a PDMS/glass hybrid microfluidic platform (Fig. 1(b)) is used which is fabricated using photolithography and soft lithography techniques.[52] The resonant frequencies of the ultrasonic microdevices are determined through electrical impedance measurements (C-60, Impedance Analyzer, Cypher Instruments Ltd., UK). The dominant acoustic resonance modes for the glass microdevice and PDMS/glass hybrid microfluidic platform are obtained as 2.37 MHz and 2.14 MHz, respectively. The acoustic pressure (P) of the microdevice is measured through a drop-voltage analysis.[53] The fundamental resonant frequency of the PZT is 2.10 MHz and the maximum peak-to-peak voltage capacity is 200 V (AC). The operating frequencies are 2.17 MHz and 2.37 MHz, respectively, which are no more than 15% of the resonance frequency of the PZT. The cell viability data (see Fig. 1 in the supplementary material[54]) also reflect that the effect of these operating frequencies is not detrimental to the live cells. The ambient temperature is maintained at 23 °C throughout the experiments.

C. Microbubble-clusters formation and characterization

In our experiments, we have used Optison Contrast Agents as ultrasonic microbubbles that belong to the class of second-generation contrast agents. It is composed of perflutren gas microbubbles coated by human serum albumin monolayer shell of thickness approximately 15 nm. The size distribution of microbubbles ranges 2.0–4.5 μm, with a total number of $5.0–8.0 \times 10^8$ microbubbles ml^{-1}. Prior to the experiments, Optison microbubbles are suspended in freshly prepared phosphate buffer saline (PBS) solution at a concentration of 5×10^6 microbubbles ml^{-1} and injected into the microdevice. The visualisations of the microbubble-clusters (MCs) formation and their dynamical motions inside the microdevice are performed under a phase-contrast

microscope (IX71 Olympus, USA) coupled with a high speed camera. The images are captured at regular interval of 50 ms. Further, the images are analysed in MATLAB software.

D. Preparation of cells for experimental studies

H9c2 cardiomyoblast cells (American Type Culture Collection, USA) are selected as a representative biological model to investigate sonoporation of suspended cells within our microdevice in presence of microbubbles and fluid flow. H9c2 cells are routinely cultured in DMEM culture medium supplemented with 10% (v/v) heat-inactivated fetal calf serum (FCS) and 100 U/ml penicillin, 100 μg/ml streptomycin, and 2 mmol/l L-glutamine. Cells are maintained in a cell culture incubator supplemented with 37 °C, 5% CO_2 in air and with 95% humidity. At about 70% confluency, H9c2 cells are harvested and cell viability is determined by trypan blue exclusion. Cell concentration is determined by means of a haemocytometer prior to the experimental studies.

E. Ultrasonic microbubble-cluster induced propidium iodide uptake

Before the experiment, H9c2 cardiomyoblast cells are suspended in phosphate buffer saline (PBS) solution after centrifugation to obtain a concentration of 2.0×10^6 cells/ml. Optison microbubbles are dissolved in the PBS solution containing cells in a ratio of 200:1, i.e., for establishing sonoporation in the suspended cells, an average concentration of 200 microbubbles/cell is added to the cell suspension. 5 μl of PI is added to the solution which acts as the probe to detect the extent of sonoporation of the cells. PI uptake of cells is established under continuous-flow with inlet flow rates (Q_{in}) ranging from 5 ml/h to 40 ml/h (typical to that of the physiological conditions) at 5, 10, 15, and 20 peak-to-peak voltage (Vp-p) under pulsed ultrasound at a resonance frequency (f) of 2.37 MHz with 1 ms pulse and 50% duty cycle, in presence of microbubbles. For each amplitude, 1 ml of cell suspension is collected in individual sterile flask and dispensed (200 μl $\times$ 5 repeats) with a multichannel pipette into corresponding rows of the microtiter well plate and the fluorescence intensity ($\lambda_{exc} = 485$ nm, $\lambda_{em} = 510$ nm) is quantified using a FLUOstar Omega plate reader and data were processed by using Omega v. 1.20 and Mars Data Analysis v. 2.00. Each experiment is repeated several times for representation of the average intensity of the spectrophotometric readings and the standard deviation. Additionally, acoustic pressure levels employed in the present study fall into the range of acoustic pressure to which microbubbles are exposed *in vivo*.[55] The continuous-flow configuration is particularly advantageous for processing large numbers of cells compared with microinjection and laser configured systems, in which only single cells or low number of cells could be processed.[56]

IV. RESULTS AND DISCUSSION

A. Standing wave resonance modes

The standing wave is established in the fluid contained in the microdevice when the input frequency would satisfy Eq. (4). The wavelength of sound (λ) may be estimated from the frequency as $v = \upsilon\lambda$, where v is the velocity of sound in water and υ is the input frequency. With the velocity of sound as 1497 m/s and maximum frequency used in this study as 3.00 MHz, the minimum wavelength may be obtained approximately as 500 μm. For the case of PDMS/glass microfluidic device, two different walls in the z direction (soft and hard) would require the standing wave to be formed with the criterion $n_z\lambda/4 = h$. As the channel heights are less than the minimum wavelength required to form a standing wave ($\lambda/4$), the resonance mode in z-direction (n_z) is always zero. There are no pressure nodes possible in z-direction except at the channel wall which would impose $p = 0$ owing to the soft wall boundary condition of PDMS. On the contrary, for the glass microdevice (with both hard walls), the standing wave could be formed with $n_z\lambda/2 = h$, and as the height of the glass microdevice is 300 μm, the fundamental mode could exist in the z direction ($n_z = 1$). Different resonance modes are established in x and y directions in the microdevice satisfying the criteria $n_y\lambda/2 = w$ and $n_x\lambda/2 = l$ for both the

cases. With $l = 2.5$ cm and $w = 2$ mm, different resonance modes are obtained from Eq. (4). The first resonance mode in x and zeroth mode for y may be obtained as $f_{100} = 29$ kHz, while the first resonance mode in the y-directions may be obtained as $f_{010} = 374$ kHz.

B. Formation of microbubble-clusters

When a standing wave is established, the microbubbles experience primary Bjerknes force which directs it towards the nodes or antinodes depending upon the excitation frequency. As the microbubbles translate in the medium towards a fixed point, it experiences secondary Bjerknes force from other microbubbles in the medium. In this process, a group of microbubbles aggregate to form a "cluster." The size of clusters may depend upon the size of the individual microbubbles, input acoustic frequency, concentration of microbubbles, and confinement or properties of the walls. The microbubble-clusters act as a single entity and oscillate in the acoustic medium. Upon switching off the ultrasound, the microbubble-cluster isolates into individual microbubbles. The reversible and repeatable nature of formation of microbubble-clusters may be exploited towards tuneable sizes of microbubble-clusters for several applications of encapsulation or drug delivery.

We have observed microbubble-clusters as a function of the input frequencies of the acoustic wave in different microfluidic device configurations (height 50 μm, 75 μm, and 100 μm). The microbubble-clusters may be observed in Fig. 2(a) for 1.93 MHz (as a representative case) in a 100 μm (height) microdevice. The microbubble-clusters are encircled as red. The location of the clusters gives indication of the nodes of the standing waves. The clusters are not stationary and oscillate under the effects of the ultrasound. The distance between the clusters changes with the input frequency because the nodes are established as governed by the wavelength of the standing wave. The image is processed by subtracting the background and subsequently creating a binary mask of the image. As the microbubbles create a distinct contrast in the image, the regions containing the microbubbles have different intensity thresholds. The boundary of the microbubble-clusters is identified. The diameter of the clusters is calculated as a function of input acoustic frequencies and plotted in Fig. 2(b) for different heights of the microdevice. It may be observed that at low acoustic frequencies (<1 MHz) there is a wide scatter in the radius of the microbubble-clusters and no consistent trend could be observed. It may be noted here that the microbubble-clusters are not stationary in space. The isolated microbubbles travel towards the big microbubble-clusters if they are left for long time under the influence of acoustic stimulation. Slight perturbations lead to creation of the gradient of the acoustic pressure and

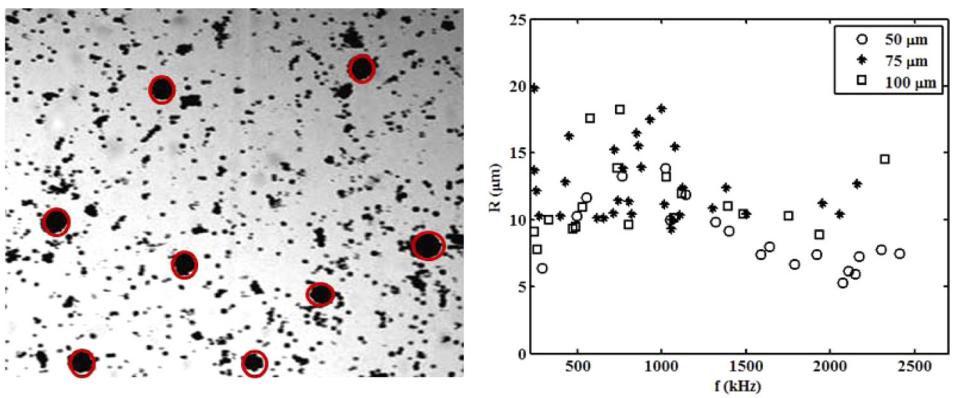

FIG. 2. (a) The microbubble-clusters established at 1.93 MHz in 100 μm PDMS/glass hybrid microdevice with microbubble concentration 5% (v/v) in aqueous solution (clusters are marked by red circles). The snapshot represents only a transient where isolated microbubbles are yet to reach the big microbubble-cluster. (b) The variation of the average microbubble-cluster as a function of the input frequency for different microdevice configurations (heights 50 μm, 75 μm, and 100 μm).

exerting forces on the microbubble-clusters make the clusters oscillate in the flow. More dynamical aspects of the clusters would be discussed in Section III C. The snapshot in Fig. 2(a) represents only an instantaneous configuration of the microbubble-clusters. As the frequency is increased (closer to the dominant resonance frequency of 2.14 MHz), the scatter decreases and at the same time the diameter of the microbubble-cluster decreases. The acoustic streaming of the microbubble-clusters is faster near resonance frequencies because at these frequencies, the effects are the strongest, and the average radius of these clusters is narrowed down to few values (less spread in the data). The average radius of microbubble-clusters over the range of frequencies may be obtained to be 12 μm. The heights of the microdevice have marginal effect on the resonance frequencies, and hence the diameter of microbubble-clusters remains mostly unaffected by changing the confinement levels.

C. Dynamical aspects of microbubble-clusters

Although the microbubble experiences a force towards a node, all the microbubbles should accumulate at fixed points (nodes) in the ultrasonic microdevice. The accumulated microbubbles would form an aggregate in the form of a stable "cluster" at the nodes as described in Section III B. In practice, the microbubble-clusters are not static and display a plethora of dynamic behaviour in the fluid. There are three types of motion observed in such microfluidic system—(a) translation/rotation of clusters, (b) oscillation of the clusters, and (c) interaction of cluster with biological cells.

1. Translational/rotational motions of microbubble-clusters

If a stationary microbubble-cluster is formed, it would experience a force directed towards the centre. If the cluster size is large, the force on the cluster is not uniform because of the pressure gradient created by the standing wave. The edges of the microbubble-cluster experience large forces in comparison to the centre considering the cluster is located at the node. The asymmetric force on the cluster makes the microbubble-cluster to rotate about its centre. A more general case is that the cluster when it is formed by aggregation of the microbubbles is not stationary but develops momentum while it is formed. The force acting upon the cluster is proportional to the gradient of pressure. The solution of Eq. (3) may be obtained by imposing a boundary condition of soft walls in x and y directions as $p_1 = \sin(k_x x)\sin(k_y y)\alpha(z)$, where $\alpha(z)$ represents the solution of the pressure in the z-direction and $k_x = n_x \frac{\pi}{l}$ and $k_y = n_y \frac{\pi}{w}$ are the wave-numbers with modes n_x and n_y in corresponding x and y directions. When a standing wave is established at higher modes, different compartments are formed around each node. The size of the compartment is dependent upon the resonance modes (n_x, n_y) in different directions. At higher frequency, the size of the compartment formed is small and consequently the radius of the circle of rotation of the microbubble-cluster is also small. As the radius of the circle is small, the angular frequency of rotation of the microbubble-cluster is high, which implies directly from the conservation of momentum (force between two microbubble-clusters is equal and opposite). In the limiting case, when the frequency is very high, the radius of the circle is so small (comparable to the size of the cluster), the microbubble-cluster gets directed to the node and rotates in a circular motion about its own geometrical centre of the microbubble-cluster. The gradient of the pressure represents the direction of the force as may be observed in Fig. 3(a). The contours of the magnitude of the force are superposed in the same figure. If the velocity is oriented in a direction perpendicular to the line joining the cluster and the node, the cluster moves in a circular motion. Depending upon the location of the formation of the cluster, the cluster may end up in revolving with different radius in different compartments. If two or more clusters end up in a compartment, then either they may come closer together to form a bigger cluster or they may end up in establishing equilibrium by revolving around a same node as shown in Fig. 3(b). While clusters rotate in circles, the centrifugal force tends to pull apart the microbubbles from the cluster. As a result, the cluster readjusts its position to a new radius of rotation. In Fig. 3(c), it may be observed that two microbubble-clusters rotate about a

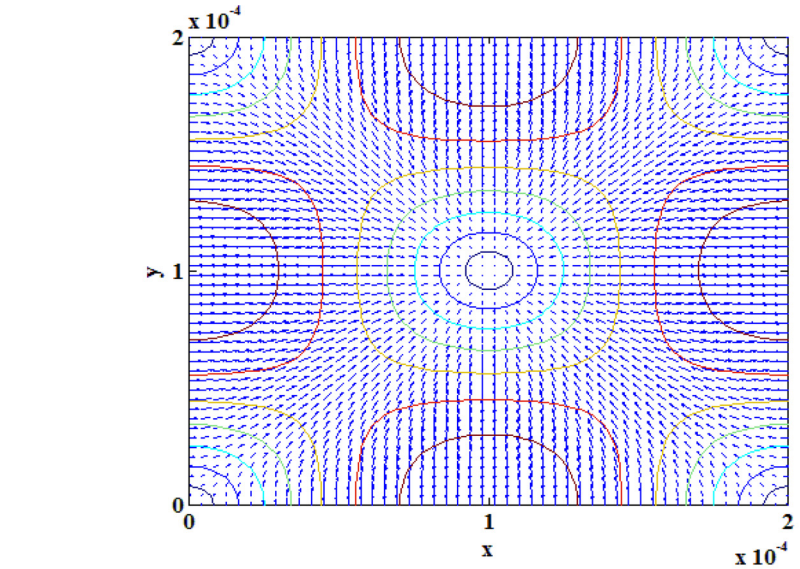

(a)

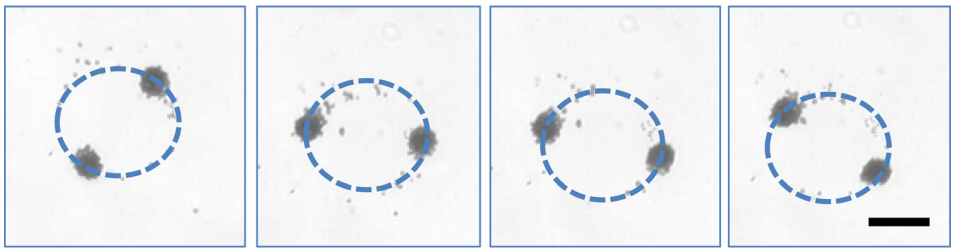

(b)

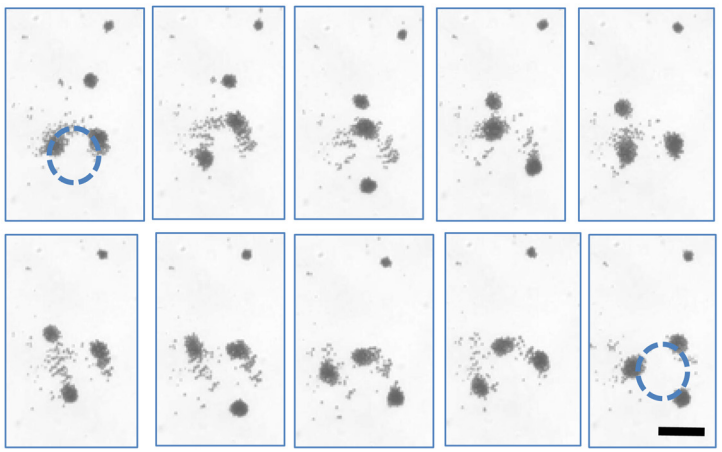

(c)

FIG. 3. (a) The direction of the force on a microbubble-cluster and the contour of the constant magnitude of force in one compartment with equal size length and width directions. The rotation of (b) two microbubble-clusters and (c) three microbubble-clusters about a node in a microdevice with height 50 μm and width 2 mm at input acoustic frequency 1.243 MHz. The representative images are at a time interval of 1.5 s (interval of three frames/snaps) for 1.243 MHz acoustic frequency. Scalebar represents 20 μm.

common centre of rotation. While rotating, some of the microbubbles come out of the clusters which result in the change in the size of the clusters. A third cluster gets attracted towards this two cluster system. Finally, at equilibrium these three clusters rotate again about the same axis.

2. Oscillations of microbubble-clusters

In addition to the translation or rotation of the microbubble-clusters, isolated microbubbles as well as the microbubble-clusters respond to the external pressure field using volume pulsations or oscillations. The nature of the oscillations may be linear to non-linear depending upon the magnitude of the acoustic field developed. The oscillation of the microbubble (or the clusters) is also governed by the surrounding medium properties, resonance frequency, damping coefficients, the radius of the microbubble (or cluster), the properties of the gas contained in the microbubble, and the shell properties of the microbubbles. Low amplitude oscillations can be described using a linearized framework (see supplementary material[54]); however, for high amplitude oscillations, we need to resort to the full non-linear equation describing the oscillations of the microbubble-clusters.

The damping coefficient is a function of the shell surface viscosity κ_s which is not known for the microbubble-cluster. The other property called the shell surface elastic modulus χ may be determined from first principle. The values of the parameters used of the calculation are—the density (ρ_L) and viscosity (μ_L) of water as 1000 kg/m^3 and 0.001 Pa s, respectively, shell surface elasticity (χ) as 0.54 N/m, the atmospheric pressure (P_0) as 101.3 kPa, the acoustic pressure P_m as 0.3 MPa, and the ratio of specific heats of gas (γ) as 1.056. The resonance frequency of the microbubble-cluster depends upon the size of the cluster (see Eq. (7) in the supplementary material[54]) and plotted in Fig. 4(a). It also depends upon the resonance frequency of a single microbubble (Optison Contrast Agent) which is close to 1.00 MHz, which decreases as several microbubbles form clusters. The resonance frequency corresponding to the average radius of the cluster (12 μm) is obtained as 240 kHz. As described earlier, when the microbubbles are excited above the resonance frequency it tends to go towards the nodes, while it reverses its direction if excited below resonance. All the subsequent analyses have been performed at input frequency above this frequency, i.e., 240 kHz. The functional dependence of the maximum shear stress on the acoustic frequency may be observed in Fig. 4(b). As we reduce the parameter δ_0, the value of the maximum shear stress increases. The value of the radius of the cluster is chosen as the average radius of the clusters as 12 μm. The maximum shear stress is of the order of 1 kPa for the case when the cluster is touching the cell surface; however, the magnitude of the shear stress rapidly decreases as the separation between the cell and the cluster increases. There exists a threshold shear stress beyond which the biological cells can undergo sonoporation, which is 12 Pa.[57] The shear stress as obtained from the linear analysis in the present situation is significantly higher and may be utilised for sonoporation of biological cells.

3. Interaction of microbubble-clusters with biological cells

The attraction of two compressible entities in acoustic field owing to secondary Bjerknes force needs not to be limited to the microbubbles-clusters only. The secondary Bjerknes force is proportional to the rate of change of volume which may be demonstrated by any substance which has the ability to compress. Biological cells are soft entities which respond to the external acoustic oscillations. Mechanical resonances of biological cells such as shape vibration of the red blood cells can be predicted using an oscillating bubble with resonance frequency close to that of the cell.[58] Oscillation of algae cell wall at 1.00 MHz ultrasound at resonance was observed when standing wave was established.[59] A theoretical model of the interaction of microbubbles with bacteria in the ultrasonic field was developed using a shell model of the bacteria.[60]

Under the application of ultrasound in glass microdevice (rectangular cross section with all walls made of glass—a symmetric wall condition), a standing wave is established with a nodal plane (instead of a point) through the centre of the microdevice corresponding to the first mode of excitation. When the cells are suspended in such a glass microdevice, they move towards the nodal plane. When microbubbles and the cells are inserted together into the glass microdevice, not only they tend to move towards the nodal plane but also tend to interact. Hypothetically, if the interaction of the cell and the microbubble-cluster does not exist, then the microbubble-cluster

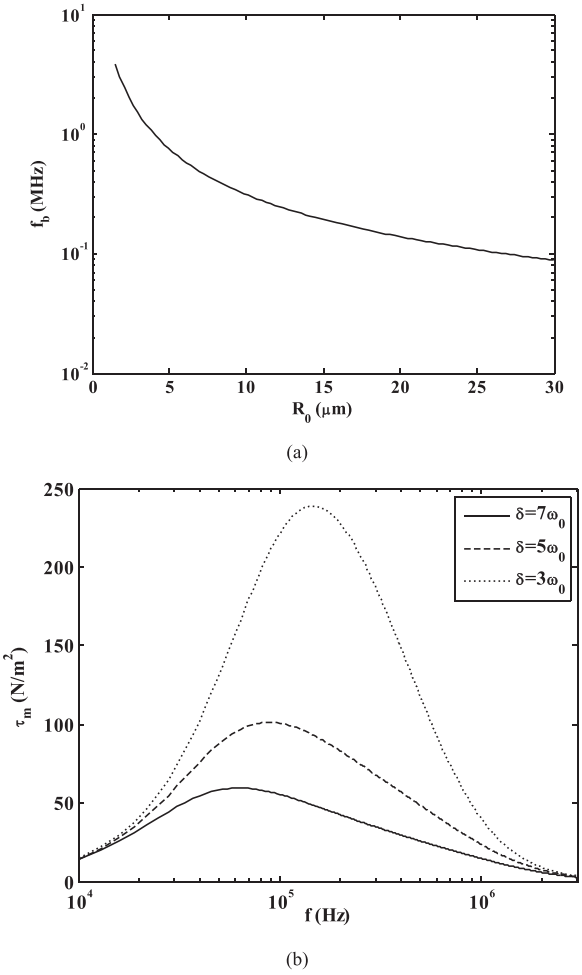

FIG. 4. (a) The resonance frequency ($f_b = \omega_0/2\pi$) of the microbubble-clusters as a function of the size of the clusters oscillating in a liquid (water) as obtained from the linearised theoretical model for oscillating microbubble-clusters. (b) The maximum shear stress as a function of the acoustic frequency ($f = \omega/2\pi$) when the microbubble-cluster is touching the cell membrane, for different values of the damping coefficient (expressed as a function of the resonance frequency ω_0).

(which would be still formed because of inter-bubble attraction in acoustic field) and the cells would rest in the nodal plane without coming closer to each other. It may be observed in Fig. 5(a) that the cells are located in the nodal plane with the microbubble-clusters attached to them. Interestingly, this phenomenon is not limited to suspended cells only.

When adherent cells are cultured in a microfluidic platform (unlike the earlier case, this is a hybrid PDMS/glass microfluidic device with three walls of PDMS and one wall of glass), the cells adhere on the glass wall of the microfluidic device unbiased, or in other words, they do not have any preferential location to adhere (although the adherence is a function of surface condition and cell-cell interactions). Unlike in the case of suspended cells, the cells do not move towards the nodal plane under ultrasound applications because they are adhered on the walls. When the microbubbles are inserted into the microdevice and ultrasound is switched on, we observe that the microbubble-clusters come in the vicinity of the adhered cells as shown in Fig. 5(b) even though the microbubble-clusters experience a strong force towards the node while the cells are not located at the nodes. This implies that the mutual attraction force between the cell and the microbubble-cluster which is secondary in nature is stronger than the primary Bjerknes force acting upon the microbubble-clusters. The primary Bjerknes force on the cells is, however, resisted or overcome by the traction force exerted by the cell adhering at the focal points on the wall. The secondary Bjerknes force is dependent upon the volume (or

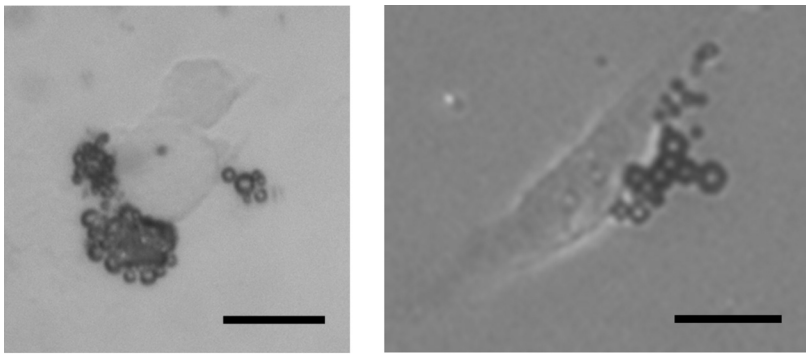

(a) (b)

FIG. 5. The microbubble-clusters accumulate close to the cells (a) suspended H9c2 cardiomyoblast cell in the glass microdevice moves towards the nodal plane at a frequency 2.37 MHz and the input acoustic voltage is 3.14 Vp-p (b) adherent cervical cancer (HeLa) cell in PDMS/glass microfluidic device adhered at the wall with microbubble-cluster in the vicinity at a frequency 2.14 MHz at 10 Vp-p acoustic input voltage. Microbubbles are added in the medium in 1:200 ratio (v/v). Microscope focus adjusted to the plane of the pressure node. Scalebar represents 10 μm.

more accurately the rate of change of the volume) of each entities. As the cell membrane can oscillate in ultrasonic field in conjunction with a microbubble-cluster of size closely comparable to the cell radius, the microbubble-cluster experiences a force towards the cell surface. The magnitude of the force as governed by the secondary Bjerknes force is proportional to $\langle \dot{V}_1 \dot{V}_2 \rangle$, where V_1 and V_2 are the volume of the microbubble-cluster and the volume of the cell, respectively, and the dot represents the rate. The force is also proportional to the inverse of the distance between them, which in this case is very low as they are virtually touching each other. Here, the radius is calculated from centre to centre, and hence the distance is not zero.

D. Sonoporation in suspended cardiomyoblast cells

The oscillating microbubble-clusters (MCs) in the vicinity of the cells in suspension impart local shear stress on the cells. In physiological conditions, the oscillating microbubble-clusters are also exposed to background flow conditions. We investigate the quantitative effects of combined shear stress generated from the background fluid flow and oscillating microbubbles-clusters on cell suspensions. We have utilised the microstreaming of the microbubble-clusters for sonoporation to quantify the uptake of small probing molecules such as PI and observed some non-trivial characteristics of uptake in presence of MCs, ultrasound and background hydrodynamic flow (pressure-induced).

1. Effects of hydrodynamic shear stress over acoustic shear stress

The phenomenon sonoporation involves the use of acoustics for modifying the permeability of the cell plasma membrane, which the hydrodynamic shear stress alone is not capable to produce the effects. We use a base acoustic pressure and vary the hydrodynamic stress over this acoustic input. The hydrodynamic shear stress may be obtained as $\tau_H = \frac{6\mu_L Q}{w^2 H}$, where Q is the input flow rate, μ_L is the viscosity of the liquid, and w and H are the width and height of the microdevice. To obtain different levels of hydrodynamic shear stress, we have varied the width of the microdevice (from 50 μm to 200 μm) and kept other parameters including the input flow rate as fixed at 3 ml/h. To reduce the variability of the experimental uncertainties, we have used a network of the microchannels for this purpose as shown in Fig. 6(a). Such microchannel network also mimics the arterial network of the heart, where the contrast microbubbles are used for echocardiography. The dominant resonance frequency is obtained as 2.17 MHz for this microchannel network and the acoustic pressure used is 0.26 MPa. The uptake of the propidium iodide (PI) dye by a single H9c2 cell from the extracellular medium has been shown in Fig. 6(b) in order to visually understand the sonoporation process in H9c2 cells. Here, the

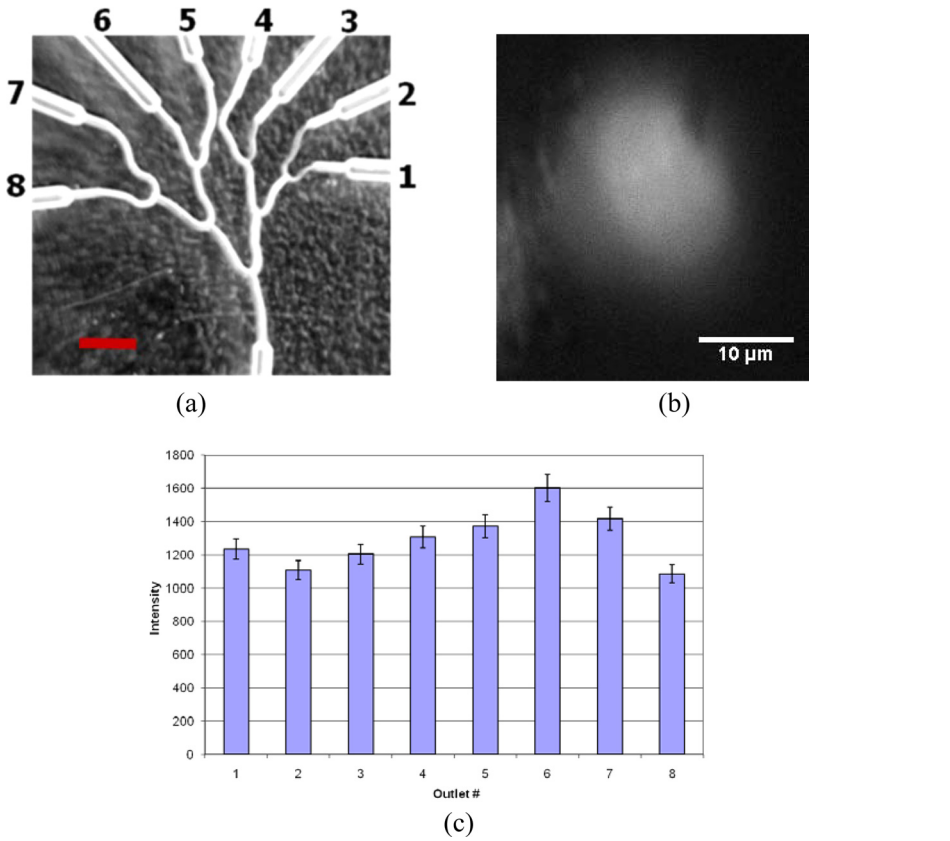

FIG. 6. (a) The network of microchannels with the width of the microchannels varying from 50 μm to 200 μm. Scalebar represents 200 μm. (b) Fluorescent image of propidium iodide (PI) uptake by a single H9c2 cell. (c) Collective fluorescence intensity of PI from the uptake by H9c2 cells via sonoporation as obtained from the spectrophotometric readings from different outlets of the microchannel network with input flow rate of 3 ml/h and acoustic input frequency of 2.17 MHz and 0.26 MPa acoustic pressure.

hydrodynamic shear stress changes 16 times in response to the change of 4 times of the width of the microchannel network. This change in the hydrodynamic stress results in 45% change in the sonoporation effect as may be observed in Fig. 6(c).

2. Combined effects of varying acoustic stress and hydrodynamic stress

We have varied both the acoustic stress and the hydrodynamic stress to investigate the combined effects of these two stresses. Different acoustic stress levels are obtained by increasing the input voltage from 5 Vp-p to 20 Vp-p which may be interpreted through the acoustic pressures in the range of 0.06 MPa–0.26 MPa. Different hydrostatic stress levels are achieved by varying the input flow rates in the single glass microdevice. We have observed that increasing the hydrodynamic shear stress with constant acoustic pressure increases the sonoporation efficiency (Section IV D 1). Different hydrodynamic stress can be also be achieved by changing the flow rates. The cells get exposed to the ultrasound effects only when they are inside the microdevice, which we define as the residence time. As we increase the flow rate, the residence time decreases, and consequently affects the sonoporation efficiency. The residence time may be estimated as l/U_{avg}, where l is the length of the microdevice and U_{avg} is the average flow velocity inside the microdevice. As the length of the microdevice is constant (=25 mm), the residence time is inversely proportional to the flow rate (or average flow velocity). We non-dimensionalise the flow rate (Q_{nd}) using the product of the maximum velocity of the microbubble-cluster in an acoustic cycle (U_m, see Eq. (5) in the supplementary material[54]) and the cross-section of the microdevice. We non-dimensionalise the residence time (t_{nd}) using a

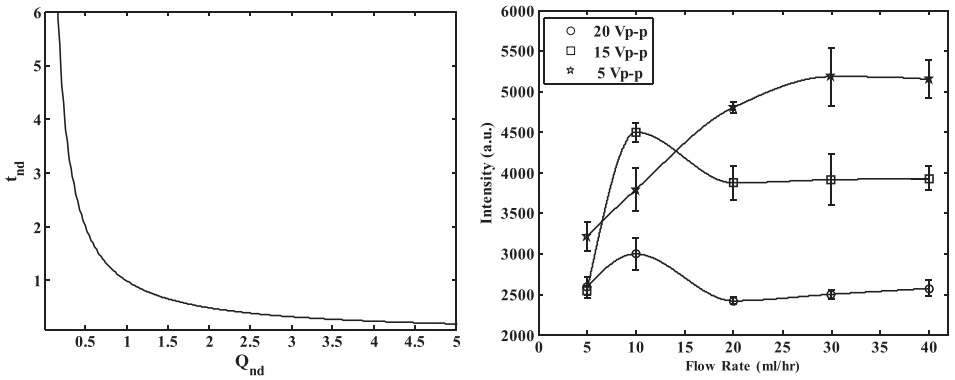

FIG. 7. (a) Variation of the non-dimensional residence time (t_{nd}) of the H9c2 cardiomyoblast cells in the microdevice as a function of non-dimensional flow rates (Q_{nd}). (b) The collective fluorescence intensity of propidium iodide (PI) from the uptake by H9c2 cells via sonoporation under different acoustic input voltages (5 Vp-p, 15 Vp-p, and 20 V p-p) and different flow rates (5 ml/h, 10 ml/h, 20 ml/h, 30 ml/h, and 40 ml/h).

time scale l/U_m. We plot the non-dimensional residence time (t_{nd}) versus the non-dimensional flow rates (Q_{nd}) in Fig. 7(a). It may be observed in Fig. 7(a) that at $Q_{nd} > 2.5$, the non-dimensional residence time (t_{nd}) almost becomes constant and goes below value 1. The combined effects of the acoustic and the hydrodynamic stresses on sonoporation, which is manifested through the intensity measurements of PI, are shown in Fig. 7(b). Higher acoustic power results in higher sonoporation. However, at low flow rates, we do not observe much variation with acoustic pressure. With the increase of flow rate, the difference between the sonoporation effect at different acoustic pressures increases. Interestingly, increasing flow rates beyond the flow rates of 20 ml/h, the sonoporation effect tends to be constant. This may be attributable towards the fact that the cells inside the microdevice do not get sufficient time to respond to the ultrasound induced perturbation for flow rates higher than 20 ml/h, as also observed in Fig. 7(a) that at such high flow rates, the residence times become constant.

V. CONCLUSIONS

In this paper, the standing waves are established in a biocompatible acoustic microdevice. A glass microdevice is considered to demonstrate hard wall condition and a PDMS/glass hybrid microfluidic device to demonstrate soft wall boundary conditions. The dominant resonance modes are obtained as 2.37 MHz and 2.14 MHz for glass microdevice and PDMS/glass hybrid microfluidic device, respectively. Microbubbles are introduced in such an acoustic environment to observe ultrasound induced clustering of the microbubble at the nodes, which is a unique feature for microfluidic systems. The size of the microbubble-clusters is determined for different microdevice heights and different acoustic frequencies. The dynamics of these microbubbles-clusters is studied using high speed imaging microscopy. It is observed that either the microbubble-clusters are stationary or they tend to orbit around the nodal points. Further, the dynamics of these microbubble-clusters is studied in the vicinity of cells. As the cells are soft entities and respond to incoming acoustic waves, the microbubble-clusters and the cells also interact with each other. This forms the basis of the cell-bubble interaction. The oscillating microbubble-clusters perturb the fluid and induce a streaming flow in the vicinity. The shear stress induced by such oscillating microbubble-clusters is estimated theoretically. Under the influence of the oscillating microbubble-clusters, the cells experience shear stress which leads to sonoporation. The combined effects of acoustic stresses and the hydrodynamic stresses are investigated by altering the width of the microdevice, flow rates, and the acoustic pressures. Future investigations may be directed towards explaining the experimental observations with

numerical simulations. Our study provides an *in vitro* strategy for targeted drug delivery and could evolve as an important clinical method for therapeutics.

ACKNOWLEDGMENTS

We would like to thank UK India Education and Research Initiative (UKIERI) for funding this research (Project No. SA08-086). We thank Dr. Debapriya Chakraborty and Dr. Dario Carugo for their assistance in experiments and manuscript preparation.

[1]R. Gramiak and P. M. Shah, Invest. Radiol. **3**, 356 (1968).
[2]F. Calliada, R. Campani, O. Bottinelli, A. Bozzini, and M. G. Sommaruga, Eur. J. Radiol. **27**, S157 (1998).
[3]M. J. K. Blomley, J. C. Cooke, E. C. Unger, M. J. Monaghan, and D. O. Cosgrove, Br. Med. J. **322**, 1222 (2001).
[4]M. Barak and Y. Katz, Chest J. **128**, 2918 (2005).
[5]S. Mitragotri, Nat. Rev. Drug Discovery **4**, 255 (2005).
[6]D. Cosgrove, Eur. J. Radiol. **60**, 324 (2006).
[7]J. L. Bull, Exp. Opin. Drug Delivery **4**, 475 (2007).
[8]S. Ibsen, C. E. Schutt, and S. Esener, Drug Des. Dev. Ther. **2013**(7), 375.
[9]M. McCulloch, C. Gresser, S. Moos, J. Odabashian, S. Jasper, J. Bednarz, P. Burgess, D. Carney, V. Moore, E. Sisk, A. Waggoner, S. Witt, and D. Adams, J. Am. Soc. Echocardiogr. **13**, 959 (2000).
[10]S. Qin, C. F. Caskey, and K. W. Ferrara, Phys. Med. Biol. **54**, R27 (2009).
[11]E. C. Unger, T. O. Matsunaga, T. McCreery, P. Schumann, R. Sweitzer, and R. Quigley, Eur. J. Radiol. **42**, 160 (2002).
[12]W. G. Pitt, G. A. Husseini, and B. J. Staples, Exp. Opin. Drug Delivery **1**, 37 (2004).
[13]K. Ferrara, R. Pollard, and M. Borden, Annu. Rev. Biomed. Eng. **9**, 415 (2007).
[14]R. Suzuki, Y. Oda, N. Utoguchi, and K. Maruyama, J. Controlled Release **149**, 36 (2011).
[15]S. R. Sirsi and M. A. Borden, Theranostics **2**, 1208 (2012).
[16]J. Ye, H. He, J. Gong, W. Dong, Y. Huang, J. Wang, G. Chen, and V. C. Yang, Front. Chem. Sci. Eng. **7**, 20 (2013).
[17]S. B. Feinstein, J. Cheirif, F. J. T. Cate, P. R. Silverman, P. A. Heidenreich, C. Dick, R. M. Desir, W. F. Armstrong, M. A. Quinones, and P. M. Shah, J. Am. Coll. Cardiol. **16**, 316 (1990).
[18]M. A. Wheatley, B. Schrope, and P. Shen, Biomaterials **11**, 713 (1990).
[19]S. H. Bloch, M. Wan, P. A. Dayton, and K. W. Ferrara, Appl. Phys. Lett. **84**, 631 (2004).
[20]F. S. Foster, P. N. Burns, D. H. Simpson, S. R. Wilson, D. A. Christopher, and D. E. Goertz, Cancer Metastasis Rev. **19**, 131 (2000).
[21]G. Korpanty, P. A. Grayburn, R. V. Shohet, and R. A. Brekken, Ultrasound Med. Biol. **31**, 1279 (2005).
[22]P. A. Frenkel, S. Y. Chen, T. Thai, R. V. Shohet, and P. A. Grayburn, Ultrasound Med. Biol. **28**, 817 (2002).
[23]M. C. Cochran, J. Eisenbrey, R. O. Ouma, M. Soulen, and M. A. Wheatley, Int. J. Pharmaceutics **414**, 161 (2011).
[24]I. Lentacker, S. C. De Smedt, and N. N. Sanders, Soft Matter **5**, 2161 (2009).
[25]P. Marmottant and S. Hilgenfeldt, Nature **423**, 153 (2003).
[26]R. J. Price, D. M. Skyba, S. Kaul, and T. C. Skalak, Circulation **98**, 1264 (1998).
[27]D. M. Skyba, R. J. Price, A. Z. Linka, T. C. Skalak, and S. Kaul, Circulation **98**, 290 (1998).
[28]M. Ward, J. R. Wu, and J. F. Chiu, J. Acoust. Soc. Am. **105**, 2951 (1999).
[29]D. L. Miller and J. Quddus, Ultrasound Med. Biol. **26**, 661 (2000).
[30]M. Ward, J. Wu, and J. F. Chiu, Ultrasound Med. Biol. **26**, 1169 (2000).
[31]A. van Wamel, K. Kooiman, M. Harteveld, M. Emmer, F. J. ten Cate, M. Versluis, and N. de Jong, J. Controlled Release **112**, 149 (2006).
[32]P. Prentice, A. Cuschieri, K. Dholakia, M. Prausnitz, and P. Campbell, Nat. Phys. **1**, 107 (2005).
[33]P. Marmottant, T. Biben, and S. Hilgenfeldt, Proc. R. Soc. London, Ser. A **464**, 1781 (2008).
[34]B. Krasovitski, V. Frenkel, S. Shoham, and E. Kimmel, Proc. Natl. Acad. Sci. U.S.A. **108**, 3258 (2011).
[35]M. Postema, S. Kotopoulis, A. Delalande, and O. H. Gilja, Ultras. Med. **33**, 97 (2012).
[36]A. Hashmi, G. Yu, M. Reilly-Collette, G. Heimana, and J. Xu, Lab Chip **12**, 4216 (2012).
[37]F. Guo, P. Li, J. B. French, Z. Mao, H. Zhao, S. Li, N. Nama, J. R. Fick, S. J. Benkovic, and T. J. Huang, PNAS **112**, 43 (2015).
[38]X. Ding, Sz.-C. S. Lin, M. I. Lapsley, S. Li, X. Guo, C. Y. Chan, I.-K. Chiang, L. Wang, J. P. McCoyd, and T. J. Huang, Lab Chip **12**, 4228 (2012).
[39]J. Friend and L. Y. Yeo, Rev. Mod. Phys. **83**, 647 (2011).
[40]H. Bruus, J. Dual, J. Hawkes, M. Hill, T. Laurell, J. Nilsson, S. Radel, S. S. Sadhal, and M. Wiklund, Lab Chip **11**, 3579 (2011).
[41]C. Zhao, Y. Xie, Z. Mao, Y. Zhao, J. Rufo, S. Yang, F. Guo, J. D. Mai, and T. Jun Huang, Lab Chip **14**, 384 (2014).
[42]H. Bruus, Lab Chip **12**, 20 (2012).
[43]H. Bruus, Lab Chip **12**, 1014 (2012).
[44]H. Bruus, *Theoretical Microfluidics*, Oxford Master Series in Condensed Matter Physics (OUP Oxford, 2007).
[45]D. Rabaud, P. Thibault, J.-P. Raven, O. Hugon, E. Lacot, and P. Marmottant, Phys. Fluids **23**, 042003 (2011).
[46]V. F. J. Bjerknes, *Fields of Force* (Columbia University Press, New York, USA, 1906).
[47]M. Minnaert, Philos. Mag. **16**, 235 (1933).
[48]T. G. Leighton, A. J. Walton, and M. J. W. Pickworth, Eur. J. Phys. **11**, 47 (1990).
[49]A. Eller, J. Acoust. Soc. Am. **43**, 170 (1968).
[50]E. A. Zabalolotskaya, Sov. Phys. Acoust. **30**, 365 (1984); A. A. Doinikov and S. T. Zavtrak, Phys. Fluids **7**, 1923 (1995); H. N. Oguz and A. Prosperetti, J. Fluid Mech. **218**, 143 (1990).
[51]R. Mettin, I. Akhatov, U. Parlitz, C. D. Ohl, and W. Lauterborn, Phys. Rev. E **56**, 2924 (1997).
[52]N. Bose, T. Das, D. Chakraborty, T. K. Maiti, and S. Chakraborty, Lab Chip **12**, 69 (2012).

[53]D. Carugo, D. N. Ankrett, P. Glynne-Jones, L. Capretto, R. J. Boltryk, X. Zhang, P. A. Townsend, and M. Hill, BioMicrofluidics **5**, 044108 (2011).
[54]See supplementary material at http://dx.doi.org/10.1063/1.4928947 for description of non-linear oscillations of microbubble-clusters and cell viability study.
[55]M. A. Hassan, P. Campbell, and T. Kondo, Drug Discovery Today **15**, 892 (2010).
[56]S. Mehier-Humbert and R. H. Guy, Adv. Drug Delivery Rev. **57**, 733 (2005).
[57]J. Wu, Ultrasound Med. Biol. **28**, 125 (2002).
[58]E. Ackerman, Bull. Math. Biophys. **19**, 1 (1957).
[59]D. L. Miller, IEEE Trans. Ultrason. Ferroelectr. Freq. Control **33**, 165 (1986).
[60]P. V. Zinin and J. S. Allen III, Phys. Rev. E **79**, 021910 (2009).